Effect of Cosolutes on the Aggregation of a Tau Fragment: A Combined Experimental and Simulation Approach

Andrea Arsiccio,[†] Xikun Liu,[†] Pritam Ganguly,[†] Steven K. Buratto,[†] Michael T. Bowers,[†] and Joan-Emma Shea*,[†],[‡]

†Department of Chemistry and Biochemistry, University of California, Santa Barbara, California 93106, United States

‡Department of Physics, University of California, Santa Barbara, California 93106, United
States

E-mail: shea@ucsb.edu

Abstract

The intrinsically-disordered protein Tau represents the main component of neurofibrillary tangles that are a hallmark of Alzheimer's disease. A small fragment of Tau, known as paired helical filament 6 (PHF6), is considered to be important for the formation of the β -structure core of the fibrils. Here we study the aggregation of this fragment in the presence of different cosolutes, including urea, TMAO, sucrose, and 2-hydroxypropyl- β -cyclodextrin (2-HP β CD), using both experiments and molecular dynamics simulations. A novel implicit solvation approach (MIST - Model with Implicit Solvation Thermodynamics) is used, where an energetic contribution based on the concept of transfer free energies describes the effect of the cosolutes. The simulation predictions are compared to thioflavin-T and atomic force microscopy results, and the good agreement observed confirms the predictive ability of the computational approach herein proposed. Both simulations and experiments indicate that PHF6 aggregation is inhibited in presence of urea and 2-HP β CD, while TMAO and sucrose stabilize associated conformations. The remarkable ability of $HP\beta CD$ to inhibit aggregation represents an extremely promising result for future applications, especially considering the widespread use of this molecule as a drug carrier to the brain, and as a solubilizer/excipient in pharmaceutical formulations

Introduction

Tau is an intrinsically-disordered, microtubule-associated protein, predominantly found in brain cells.¹ Abnormally phosphorylated Tau is the main component of neurofibrillary tangles² found in the brain of Alzheimer's patients, and this protein is also associated with many other neurodegenerative diseases, generally indicated as Tauopathies.^{3–8} Full-length Tau consists of an N-terminal domain, a proline rich region, a repeat region, and a C-terminal domain.⁹ The human nervous system contains six isoforms of Tau, which differ by two inserts near the N-terminal domain and the presence of either three (R1, R3 and R4) or

four (R1, R2, R3 and R4) imperfect repeat sequences in the C-terminal domain. $^{10-12}$ These repeat sequences play a major role in the microtubule binding ability of Tau, and also influence its aggregation propensity. The R3 repeat, in particular, is part of all six Tau isoforms, and is believed to play a critical role in inducing Tau aggregation. $^{13-17}$ For instance, R3 has been shown to self-assemble into amyloid. 18 Moreover, fragments of the Tau protein containing R3 may be originated within the human brain by endopeptidase cleavage 19 and these fragments may be crucial in amyloid core formation. Specifically, the hexapeptide VQIVYK (paired helical filament 6, PHF6), located in R3, is considered crucial for Tau fibrillation. $^{20-23}$ Cryo-EM analysis of Tau filaments isolated from Alzheimer's patients has revealed that the PHF6 sequence constitutes the first β -strand of the filament core. 24 Cross-linking mass spectrometry, recombinant protein and synthetic peptide systems, in silico modeling, and cell models have additionally shown that the PHF6 motif forms metastable compact structures with its upstream sequence that modulate aggregation propensity. 25

Studying the aggregation behavior of protein fragments, like PHF6, is of paramount importance, because in many cases only a small fragment of a large protein is involved in fibrillation and formation of the amyloid core structure.²⁶ Moreover, studying the association of such fragments can elucidate the mechanisms of amyloid formation.^{27–30} In this framework, we here study the aggregation of the PHF6 fragment of Tau. We perform molecular dynamics simulations of the aggregation process, using an atomistic representation of the peptide, and an implicit description of the solvent.

More specifically, we employ a Generalized-Born (GB) method to model electrostatic interactions,³¹ and a solvent accessible surface area (SASA) term to describe the non-polar energy of solvation in water. A newly developed approach employing an energetic contribution based on the SASA of the peptide (the MIST approach, Model with Implicit Solvation Thermodynamics³²) is used to describe the role of cosolutes in the framework of the implicit solvation model. Specifically, this SASA-based term derives from the concept of group transfer free energies (GTFE), proposed by Bolen and coworkers to describe the energetics

of osmolyte-induced protein conformational transitions^{33,34} (more details will be given in the Theoretical Background section below).

This implicit description dramatically reduces the computational cost required for a statistically relevant exploration of the conformational landscape, and the absence of viscous friction further accelerates the sampling. The simulation outputs are also compared to and validated by experimental data, including a thioflavin-T (ThT) fluorescence assay and atomic force microscopy (AFM).

Our investigation examines water as solvent, but also addresses the effect of cosolutes including urea, trimethylamine N-oxide (TMAO), sucrose, and 2-hydroxypropyl- β -cyclodextrin (2-HP β CD). The cosolute 2-HP β CD is a cyclodextrin, composed of 7 α -glucopyranose monomers bonded together to form a torus-like structure. Hydroxypropyl derivatizations are linked to the O2 atoms of the glucopyranose monomers, increasing the solubility in water and conferring amphiphilic properties. The β CD is used as excipient, drug carrier and solubilizer and has been authorized by both the FDA and EMA for the treatment of Niemann-Pick type C disease, a progressive neurodegenerative disorder characterized by the intracellular accumulation of cholesterol. The potential effect of HP β CD on Tau fibrillation is, therefore, of great interest, especially considering that this functionalized cyclodextrin is often used for drug delivery to the brain.

The other cosolutes studied in this work, urea, trimethylamine N-oxide (TMAO) and sucrose, are frequently accumulated in many organisms in response to environmental stressors. ^{40,41} These molecules are known to shift the folding equilibrium of proteins, acting either as stabilizers (TMAO, ^{42,43} sucrose ⁴⁴) or as denaturants (urea). ^{45,46} Urea is a chemical denaturant used *in vitro*, and an antagonist of TMAO. ⁴⁷ Both urea and TMAO have been shown to influence the mechanism of amyloid fibrils formation. ⁴⁸ TMAO is a gut microbial-derived metabolite, produced by the metaorganismal metabolism of dietary choline. Human gut microbial metabolites, and especially TMAO, have been shown to be correlated to Alzheimer's disease. ⁴⁹ High levels of TMAO in the plasma and cerebrospinal fluid (CSF) have been shown

to be implicated in the pathogenesis of metabolic, cardiovascular and cerebrovascular diseases.⁵⁰ CSF TMAO has been found to be higher in individuals with Alzheimer's disease compared to cognitively-unimpaired individuals, and high levels of TMAO in CSF are also associated with biomarkers of Alzheimer's pathology (e.g., phosphorylated Tau).⁵¹ For instance, reduced TMAO levels by 3,3-Dimethyl-1-butanol (DMB) treatment alleviated the cognitive and pathological deterioration in transgenic mice, thus representing a potential approach for Alzheimer's disease.⁵²

In the present work we will reveal the overall aggregation propensities of PHF6 in TMAO, sucrose, urea and HP β CD, as determined by ThT and AFM experiments. We will show that the implicit solvent molecular dynamics simulations correspond to experiments in predicting the qualitative ranking for the aggregation, suggesting that free-energy based implicit solvent simulations can be applied not only to study the conformational behavior of proteins, ³² but also to investigate aggregation phenomena. The molecular dynamics simulations additionally reveal the structures of the cluster formation at different oligomeric states of PHF6, providing mechanistic insight into the aggregation pathway.

Materials and Methods

Experimental Protocol

Peptide Synthesis and Purification

The PHF6 fragment studied in this work had the C and N termini blocked by amidation and acetylation, respectively. The presence of caps, that neutralize the molecules termini, allows a more realistic comparison to full-length Tau,⁵³ and has been shown to modulate fibrillation propensity in the case of PHF6.⁵⁴

Ac-PHF6-NH₂ was synthesized on a Fmoc-Rink amide resin (Anaspec), acetylated with acetic anhydride prior to cleavage from the resin and purified by reversed-phase HPLC (RP-

HPLC) on a semi preparative C18 column (Phenomenex) using gradients of water (0.1% v/v) TFA) and acetonitrile (0.1% v/v) TFA) to achieve a purity greater than 95% by analytical RP-HPLC. Prior to experiments, the peptide was dissolved in hexafluoroisopropanol (HFIP) to monomerize preformed aggregates, dried under vacuum for \sim 24 h and stored at -20 °C.

ThT Fluorescence Assay

ThT fluorescence assays were performed on a BioTek Synergy 2 multimode plate reader in kinetic mode for a week at 37 °C. Samples were prepared by first adding different cosolutes (i.e. 2M TMAO, 6M urea, 1M sucrose and 150mM HP β CD) and then 150 μ M Ac-PHF6-NH2 followed by 50 μ M ThT into 10 mM ammonium acetate buffer (pH = 7.4), containing 150 mM NaCl. The excitation and emission filters used were 440/30 and 485/20 nm, respectively. The photomultiplier tube (PMT) gain used was 55. Baseline correction was performed on all the data.

Atomic Force Microscopy (AFM)

Samples were prepared exactly the same as for the ThT fluorescence assay, and were incubated at 37 °C for 24 h. For each experiment 50 μ L was deposited onto freshly cleaved V1-grade mica (TedPella, Redding, CA) and dried in a desiccator. Repulsive mode was used to collect images in air on an MFP-3D Atomic Force Microscope (Asylum Research, Goleta, CA) using high-resolution silicon probe tips with a tip radius of 1 nm, a cantilever spring constant of 7 N/m, and a resonant frequency of 155 kHz (MikroMasch USA, Lady's Island, SC).

Implicit Solvent Simulations

Theoretical Background

The free energy of a solvated protein can be written as:

$$G^{tot} = E^{vac} + G^{el} + G^{np}(T) + G^{tr}(c)$$

$$\tag{1}$$

where E^{vac} is the protein's energy in vacuum, which is the sum of internal contributions (bond and angle stretching, dihedral angles interactions) and van der Waals energy terms. $G^{np}(T)$ is the non-polar solvation contribution in pure water at temperature T, i.e., the free energy of hydration for a molecule from which all charges have been removed. G^{el} is the electrostatic part, calculated as the free energy for turning on the partial charges in solution. These first three terms describe a protein in pure water. The term $G^{tr}(c)$ is used to take into account the presence of cosolutes at a concentration c, and is based on the free energy of transfer approach MIST (Model with Implicit Solvation Thermodynamics), that we recently developed. 32

The generalized Born equation⁵⁵ was employed to compute G^{el} , using the OBC(II) model³¹ to estimate the Born radii. The dielectric constant was set to 74.2, which is the value for water at 310 K according to the equations in Bradley and Pitzer.⁵⁶

Using the same nomenclature that we introduced in our previous work,⁵⁷ the effect of temperature was taken into account using the method that we referred to as 'approach 3'. Briefly, approach 3 describes non-polar effects using surface tension values that depend on temperature and amino acid type, and was developed by mining a large set of protein structure files downloaded from the PDB database. Approach 3 describes $G^{np}(T)$ as,⁵⁷

$$G^{np}(T) = \sum_{k=1}^{n_r} g_{k,sc}^{tr}(T)\alpha_{k,sc} + g_{bb}^{tr}(T)\sum_{k=1}^{n_r} \alpha_{k,bb}$$
 (2)

where the summations run over the n_r residues of the protein, and $g_{k,sc}^{tr}(T)$ and $g_{bb}^{tr}(T)$ are the amino acids side chains (subscript sc) and backbone (subscript bb) contributions, respectively.

The transfer free energy term $G^{tr}(c)$, that takes into account the effect of cosolutes, shares a similar functional form, ³²

$$G^{tr}(c) = \sum_{k=1}^{n_r} g_{k,sc}^{tr}(c)\alpha_{k,sc} + g_{bb}^{tr}(c)\sum_{k=1}^{n_r} \alpha_{k,bb}$$
 (3)

For both $G^{np}(T)$ and $G^{tr}(c)$ each contribution is weighed by the fractional solvent accessible surface area $SASA_k$ of residue k,

$$\alpha_k = \frac{SASA_k}{SASA_{k,Gly-X-Gly}} \tag{4}$$

The fractional solvent accessible surface area α_k was calculated using the fast algorithm proposed by Hasel et al.⁵⁸ The script for the computation of the fractional solvent accessible surface area, and the energetic terms $G^{np}(T)$ and $G^{tr}(c)$, is currently part of the 2.8 version of Plumed as a separate module called SASA.

Simulation Protocol

The Amber ff96 force field⁵⁹ was used to describe Ac-PHF6-NH₂, which was simulated at pH 7 (+1 charge). The AMBER 20 simulation suite⁶⁰ was used, in combination with Plumed 2.4.7.⁶¹ The aggregation of Ac-PHF6-NH₂ was simulated in water, 6M urea, 2M TMAO, 1M sucrose, and 150mM HP β CD. The water or water-cosolute solution was described implicitly, as detailed in the Theoretical Background section. The generalized Born model of AMBER 20 was used to simulate G^{el} in Eq. 1, at an effective salt concentration of 150mM, while the free energy of transfer terms $G^{np}(T)$ and $G^{tr}(c)$ were added as an external bias using Plumed. The ff96 force field, in combination with the OBC(II) generalized born model (IGB = 5) was used in this work because it was shown to offer a good balance between strand and helical conformations⁶² and was successfully applied to intrinsically disordered proteins.⁶³

The Ac-PHF6-NH₂ peptide was first energy minimized for 3000 steps using the steepest descent algorithm, and then equilibrated in implicit water at 310 K for 100 ns. An equilibrated protein structure (Figure 1a) was extracted from this 100-ns run, and used as starting configuration for the subsequent trajectories.

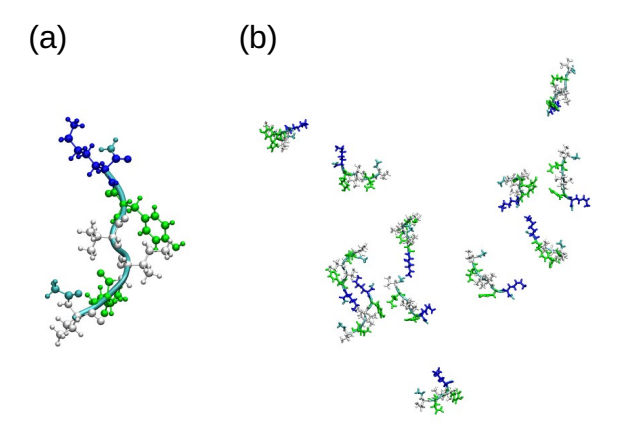


Figure 1: Starting configurations of (a) the Ac-PHF6-NH₂ peptide and (b) the 12 monomers for the aggregation study. The images were obtained using Visual Molecular Dynamics (VMD).⁶⁴ Polar uncharged residues are in green, nonpolar ones in white, positively charged in blue.

In order to study the aggregation process, 12 monomers were randomly inserted within the simulated system (Figure 1b), and were confined within a spherical cage of radius $r_{\rm sphere} = 12.4$ nm. This corresponds to a concentration of 2.5 mM, which is consistent with our previous computational investigation.⁵⁴ A harmonic potential $U_{\rm sphere}$ was used to prevent the peptides from drifting away from the spherical container,

$$U_{\text{sphere}} = \begin{cases} k_{\text{sphere}} (|\mathbf{r}_i - \mathbf{r}_{\text{center}}| - r_{\text{sphere}})^2, & \text{if } |\mathbf{r}_i - \mathbf{r}_{\text{center}}| > r_{\text{sphere}} \\ 0, & \text{otherwise} \end{cases}$$
(5)

 \mathbf{r}_i is the position of the center of mass of peptide i, while $\mathbf{r}_{\text{center}}$ is the position of the center of the sphere. k_{sphere} was set to 10 kcal/(mol nm²). Increasing the value of r_{sphere} would make the simulations extremely computationally expensive, because of the increased percentage of the configuration space corresponding to monomeric states. In any case, the magnitude of the spherical harmonic potential was small compared to the total potential energy of the system, suggesting that the results and conclusions are not affected by the specific choice of the restraining potential used. Moreover, the same sphere radius r_{sphere} was used for all the simulations, to allow a direct comparison between the different systems

investigated.

The production runs lasted 500 ns; the first 300 ns were considered as an approach to equilibration, and only the last 200 ns were used for the analyses. Convergence was assessed by monitoring the evolution of selected variables as function of simulation time, and a simulation was deemed as converged when only fluctuations around equilibrium values were observed (Figure S1). Langevin dynamics was used to control the temperature at 310 K during both the equilibration and the production runs, using a collision frequency of 1.0 ps⁻¹. The SHAKE algorithm⁶⁵ was applied to constrain all bonds linking to hydrogen atoms, and a time step of 2.0 fs was used. Configurations were saved every 2 ps, and the center of mass translation and rotation were removed every 500 steps (1 ps). No cut-off was used for the Coulombic and Lennard-Jones interactions.

The $g_{k,sc}^{tr}(T)$ and $g_{bb}^{tr}(T)$ values (to be inserted into Eq. 2) for a temperature of 310 K were obtained from our previous work of temperature-induced conformational transitions in implicit solvent⁵⁷ and are listed in Table S1. The $g_{k,sc}^{tr}(c)$ and $g_{bb}^{tr}(c)$ values (to be inserted into Eq. 3) for the different cosolutes considered in this work (urea, TMAO, sucrose and HP β CD) were taken either from the work by Bolen and coworkers ^{46,66-68} and Moeser and Horinek, ⁴⁵ or from our computational investigation of HP β CD, ⁶⁹ and are listed in Table S2.

Analysis of the Trajectories

Secondary structure content

The secondary structure during the equilibrated trajectories (last 200 ns) was analyzed using the STRIDE algorithm,⁷⁰ as implemented in the Timeline tool of VMD.⁶⁴ The fraction of time that each residue of PHF6 was found in a given configuration (α -helix, β -sheet, turn, coil etc.) could therefore be computed.

Hydrogen bond analysis

The number of hydrogen bonds within each system was also measured. To determine the presence of a hydrogen bond, a geometrical criterion was used, requiring that the distance between donor and acceptor was less than 0.30 nm, and that the angle formed between the acceptor, hydrogen and donor atoms was greater than 135°.

Results and Discussion

Experimental Results Indicate that TMAO and Sucrose Foster PHF6 Aggregation, while Urea and HB β CD Promote the Monomeric State

To compare the aggregation propensity of PHF6 under different solution conditions, we monitored the fibrillation kinetics for a week using thioflavin T (ThT) amyloid marker (Figure 2). PHF6 in both 2M TMAO and 1M sucrose exhibited an immediate increase in ThT fluorescence intensity with no lag phase, while PHF6 in 6M urea and 150 mM HP β CD buffer solution showed no increase within 1 week. PHF6 in the buffer had a lower intensity and longer lag phase than in sucrose and TMAO. All these results indicate that TMAO and sucrose promote aggregation while urea and HP β CD suppress aggregation.

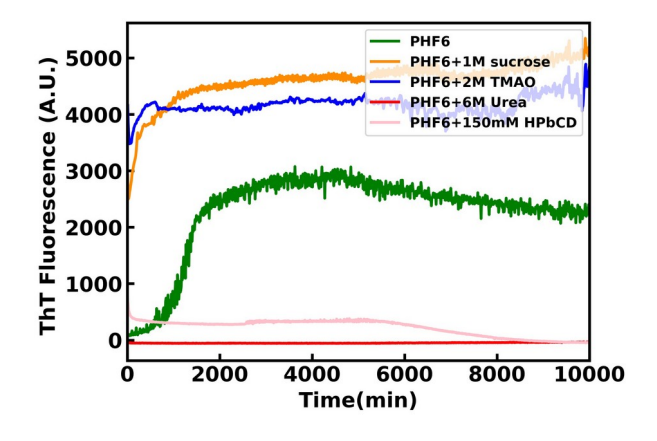


Figure 2: ThT fluorescence for PHF6 in 2M TMAO (blue) and in 1M sucrose (orange) showed an immediate and higher increase than PHF6 in buffer (green), while PHF6 in 6M urea (red) and in 150 mM HP β CD (pink) showed no increase within 1 week.

AFM Data Indicate that PHF6 Forms Aggregates with Different Morphology in Different Cosolutes

AFM studies were used to determine whether cosolutes affect fibril morphology. PHF6 in buffer solution forms mostly short fibrils (Figure 3A). However, in 1M sucrose, disordered aggregates were observed on top of a film of ribbon-like aggregates (Figure 3B). Long fibrils were formed in the 2M TMAO solution which demonstrates TMAO accelerates aggregation (Figure 3C). In 6M urea, there were no fibrils and only small aggregates were observed on top of a needle-like peptide film (Figure 3D). In 150 mM HP β CD, only a disordered peptide film was observed (Figure 3E). These results indicate that urea and HP β CD suppress PHF6 aggregation, which is consistent with the ThT fluorescence results. These AFM data show that the fibril morphologies in the presence of cosolutes are different from what is observed in pure buffer, suggesting that the cosolutes may affect the extent and morphology of fibrillation.

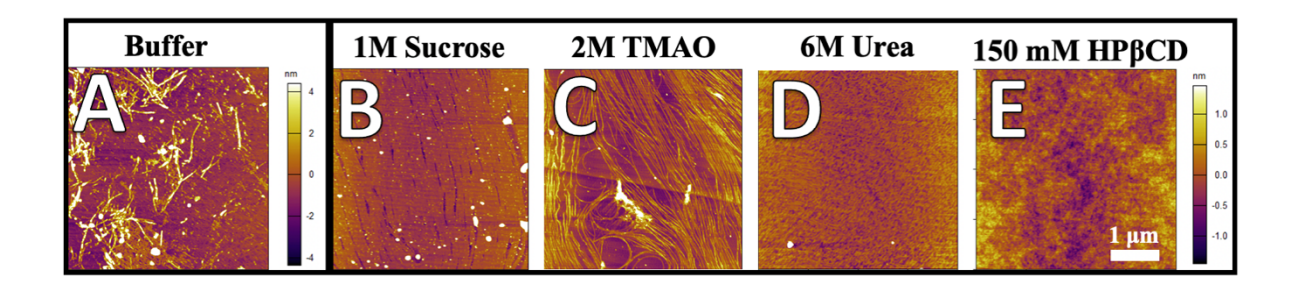


Figure 3: AFM images of PHF6 with fibrils and oligomers features in different solution conditions: (A) PHF6 in buffer solution shows short fibrils, (B) PHF6 forms granular aggregates on top of ribbon-like aggregates in the presence of 1M sucrose, (C) PHF6 in 2M TMAO solution forms long fibrils, (D) PHF6 forms small aggregates on top of an ordered peptide film in urea solution, (E) PHF6 in HP β CD is fully disordered, with no signs of fibril formation. Each image is $4 \times 4 \ \mu m^2$ with a scale of 1 μ m shown in the lower right-hand corner. Image A has a height scale from -4 to 4 nm, and images B-E from -1 to 1 nm, where lighter colors correspond to taller features.

The Transfer Free Energy-Based Simulations Predict the Aggregation Behavior of PHF6 in Different Solution Conditions

The effect of cosolutes is taken into account in our implicit solvent simulations by means of a free energy of transfer term, ^{33,67} according to the MIST protocol. ³² Using this simulation approach, we quantified the aggregation propensity of PHF6 in the different solution conditions studied in the present work.

The average number of hydrogen bonds and of contacts between the PHF6 molecules were computed during the equilibrated (last 200 ns) trajectories (Figures 4a,b). The latter quantity was defined as the number of N-C $_{\alpha}$ -C atoms of one peptide that were closer than 0.6 nm to the N-C $_{\alpha}$ -C atoms of the other peptides. The average solvent accessibility of the backbone atoms (SASA $_{bb}$) was also evaluated during the last 200 ns of each trajectory (Figure 4c). Errors were estimated by block averaging. Briefly, the equilibrated trajectories were divided into 4 blocks, and the standard deviation computed over the average values of the properties in each of the blocks.

We observed that capped PHF6 aggregated in water (\pm 150 mM salt) in our simulations. The 12 peptides formed, on average, 14.0 ± 0.6 hydrogen bonds and 107 ± 4 contacts between each other in these conditions. In the presence of 2M TMAO the number of hydrogen bonds grew to 18.0 ± 0.6 , and the number of contacts to 132 ± 6 . Such an increase in aggregate formation was accompanied by a decrease in exposure of backbone atoms (from 13.6 ± 0.4 nm² in water to 11.2 ± 0.4 nm² in TMAO), in line with the positive value of $g_{bb}^{tr}(c)$ for TMAO (0.753 kJ mol⁻¹, see Table S2).

A similar effect was noted upon addition of 1M sucrose. The number of hydrogen bonds increased to 23 ± 1 . The number of backbone-backbone contacts was also very high when the presence of the disaccharide was considered in the simulations, and the exposure of backbone atoms correspondingly decreased compared to water.

For the specific case of urea, two different sets of transfer free energies have been proposed in the literature, by Auton, Holthauzen and Bolen⁴⁶ (urea-b) and Moeser and Horinek⁴⁵

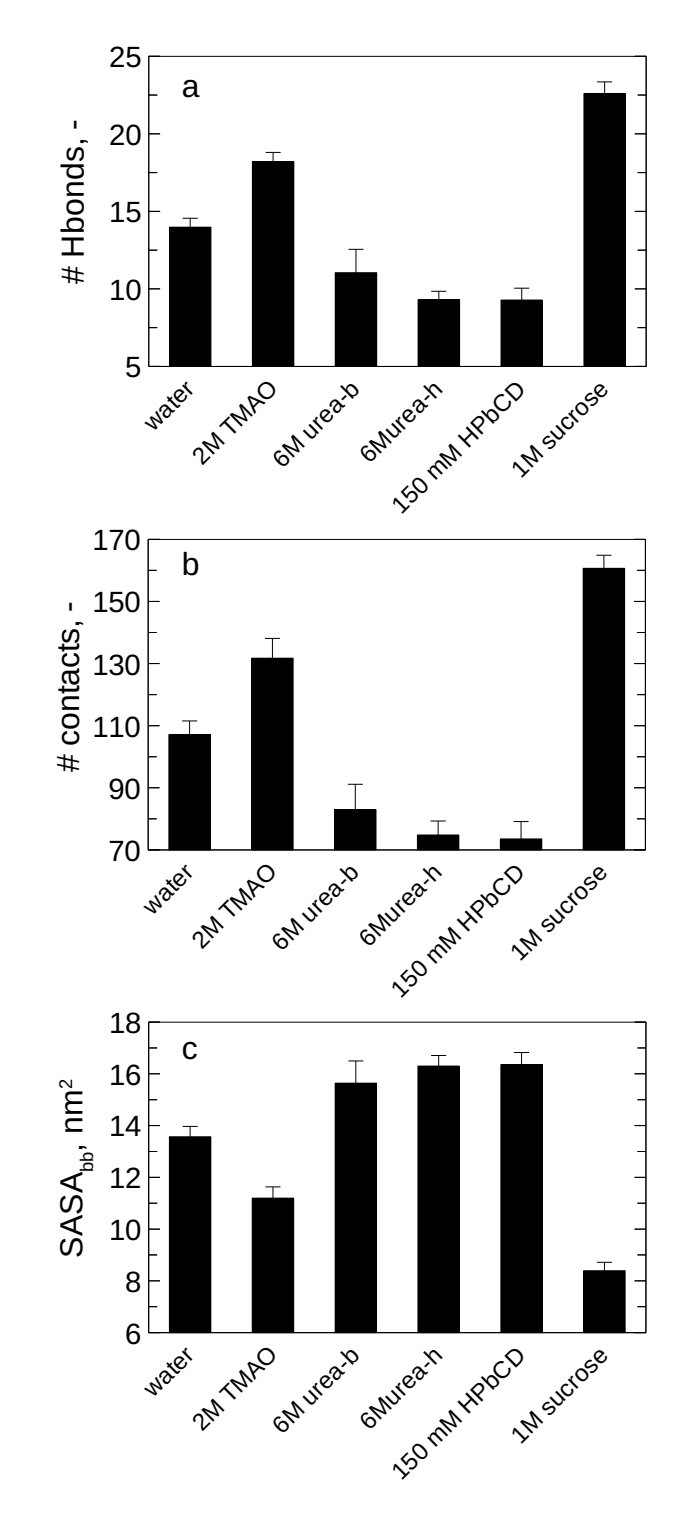


Figure 4: Average number of (a) interpeptide hydrogen bonds or (b) backbone (N-C $_{\alpha}$ -C)-backbone contacts, and (c) average solvent accessibility of the backbone atoms SASA $_{bb}$, for the different systems studied. Error bars show one standard deviation, as estimated by block averaging.

(urea-h). We showed in our previous work³² that these two descriptions of urea result in the prediction of different mechanisms for the effect of urea on protein behavior, with the Bolen set predicting strong urea-backbone interactions, and the Horinek set ascribing equal importance to both the urea-backbone and urea-sidechain interactions. We tested both the experimental sets of transfer free energies on the aggregation of PHF6 in this work (Figure 4), and observed that their predictions of aggregation propensity are very similar. The number of contacts decreased to 83 ± 4 (for 6M urea-b) or 75 ± 8 (for 6M urea-h), and the exposure of backbone atoms was greater than in water for both sets of transfer free energies (15.6 \pm 0.3 nm² for urea-b and 16.3 \pm 0.6 nm² for urea-h). The Horinek description is likely to be more accurate, as it corrects for two errors that were made in the derivation of the Bolen model. For this reason, and considering that both sets predict a similar extent of PHF6 aggregation, we will focus our attention on the urea-h set in the remainder of this work.

For HP β CD, we obtained the transfer free energy values from our prior computational work, ⁶⁹ as detailed in Supporting Information. The force field employed for HB β CD in our previous work was based on the ADD description for sugars, ⁷¹ that was developed with the specific aim to guarantee a reliable prediction of transfer free energies in ternary proteinwater-cosolute mixtures. This should ensure a correct evaluation of the $g_{k,sc}^{tr}(c)$ and $g_{bb}^{tr}(c)$ values used for HP β CD in the MIST approach. Using these transfer free energies, we found that HP β CD inhibits PHF6 aggregation. The number of contacts decreased to 74 ± 6 in 150 mM HP β CD compared to 107 ± 4 in water, and the exposure of backbone atoms was greater in these conditions (16.4 ± 0.5 nm² for HP β CD compared to 13.6 ± 0.4 nm² in water).

Special attention should be given to the results obtained for $HP\beta CD$ in this work. They are potentially relevant for future applications, because $HP\beta CD$ is a biologically safe material already employed as a drug carrier to the brain, as well as a therapeutic in the treatment of a neurodegenerative disorder (the Niemann-Pick type C disease).

The results of the implicit solvent simulations are in agreement with the preferential exclusion theory, 72 according to which protecting cosolutes, like TMAO and sucrose, should

be excluded from the protein, promoting states with reduced surface area, like the native fold. The opposite occurs in the case of denaturants, like urea, that preferentially accumulate around the peptide/protein and favor expanded structures. This preferential exclusion/interaction property also has an effect on the aggregation behavior. Stabilizing cosolutes (like TMAO and sucrose, that display a positive value of $g_{bb}^{tr}(c)$) tend to reduce the exposure of surface area and thus promote aggregation. In contrast, denaturing species like urea and HP β CD (that display a negative $g_{bb}^{tr}(c)$) increase the exposure of surface area and thus favor the monomeric state.

It is also important to note that the simulation results match the experimental data (Figure 2) in predicting the aggregation propensity of PHF6 in the different solution conditions herein investigated. As will be discussed in the next section, molecular simulations have the additional advantage of providing mechanistic insight into the pathway of aggregate formation, and of revealing the structure of PHF6 oligomers.

Molecular Simulations Provide Insight into the Oligomeric Structures of PHF6 along the Aggregation Pathway

We evaluated the average number of PHF6 clusters vs. cluster size, as observed during our simulations (Figure 5).

We found that TMAO and sucrose fostered the formation of high order aggregates (especially 8-mers for TMAO, and 11-mers for sucrose), while urea and HP β CD strongly favored the monomeric, or dimeric state. Again, the urea-h (Figure 5) and urea-b (Figure S2) descriptions predicted a similar extent of PHF6 aggregation.

The structure of the aggregates formed during the different simulations was also studied. The number of interpeptide hydrogen bonds between each residue pair was determined (Figure S3), and the secondary structure content of PHF6 computed (Figure S4).

The hydrogen bonding maps (Figure S3) suggest a predominantly antiparallel alignment of PHF6 peptides within the aggregates in 6M urea and 150 mM HP β CD, while the parallel

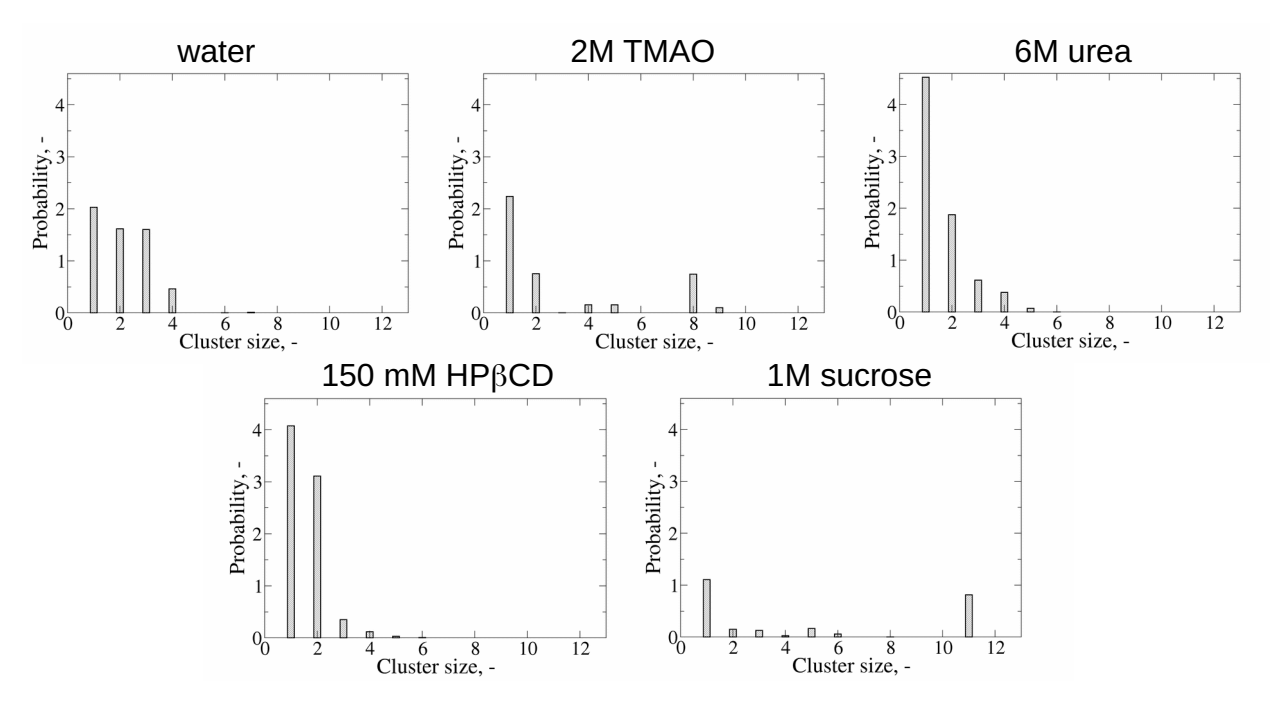


Figure 5: Average number of PHF6 clusters vs. cluster size, as observed for all the solution conditions considered. The set of transfer free energies proposed by Moeser and Horinek⁴⁵ was used for urea.

orientation is also possible in 2M TMAO and 1M sucrose. The highest number of hydrogen bonds is formed, generally, for the residues along the diagonal or codiagonals of the maps. In 2M TMAO and 1M sucrose, a non negligible number of bonds is additionally formed between the glutamine residues of two peptides, or between the isoleucine of one peptide and the glutamine of another one. The number of hydrogen bonds was, in contrast, appreciably reduced in 6M urea.

The secondary structure content of the peptides mostly corresponds to a β -sheet or a coil (Figure S4), and to a lower extent a turn may be formed, especially in water. The residues mostly involved in the formation of β -sheets are the central glutamine, isoleucine, valine and tyrosine. In line with previous observations on the extent of aggregation, TMAO and sucrose increase the β -sheet content in the simulations, while urea and HP β CD favor a coil conformation.

The radius of gyration R_q of the clusters vs. cluster size N was plotted in double loga-

rithmic scale, and fit using Eq. 6 (Figure S5),

$$R_q = AN^m (6)$$

where A is a prefactor, and the exponent m is linked to the fractal dimension d_f of the clusters 73,74 as $m=1/d_f$. The results of this analysis indicate that in all cases the growth of the cluster radius was initially characterized by a small value of m and a correspondingly high fractal dimension, which suggests spherical growth. Above a system-dependent threshold (generally $N>4\div 5$), a discontinuity was observed. The cluster growth proceeded more quickly with the addition of new monomers (higher value of m), which is indicative of an increased tendency towards linear growth. This is important, as it suggests that the aggregation pathway of PHF6 may be characterized by a first nucleation phase, followed by a linear growth towards a fibril structure.

These results are in line with previous observations, 54 and agree also with the evolution of asphericity (Figure S6). The asphericity D is defined as

$$D = 1 - 3\frac{\min(R_1, R_2, R_3)}{R_1 + R_2 + R_3} \tag{7}$$

where R_1 , R_2 and R_3 are the radii of gyration along the principal axes of the aggregates. A value of D=0 corresponds to a spherical cluster, while D=1 indicates a linear growth. Figure S6 shows that, for all the solution conditions studied, the asphericity decreased from N=1 to $N \leq 4 \div 5$, but generally increased afterwards, suggesting that the growth starts to be linear only above a given threshold of cluster size.

Finally, snapshots of the most probable conformations of each cluster are shown in Figure 6.

For small values of $N \leq 4$ growth occurred with a semi-planar geometry, while the β -sheet structure started to be distorted at N = 6. Above N = 7, the clusters assumed a cylindrical shape. These considerations are in line with our previous work.⁵⁴ As already

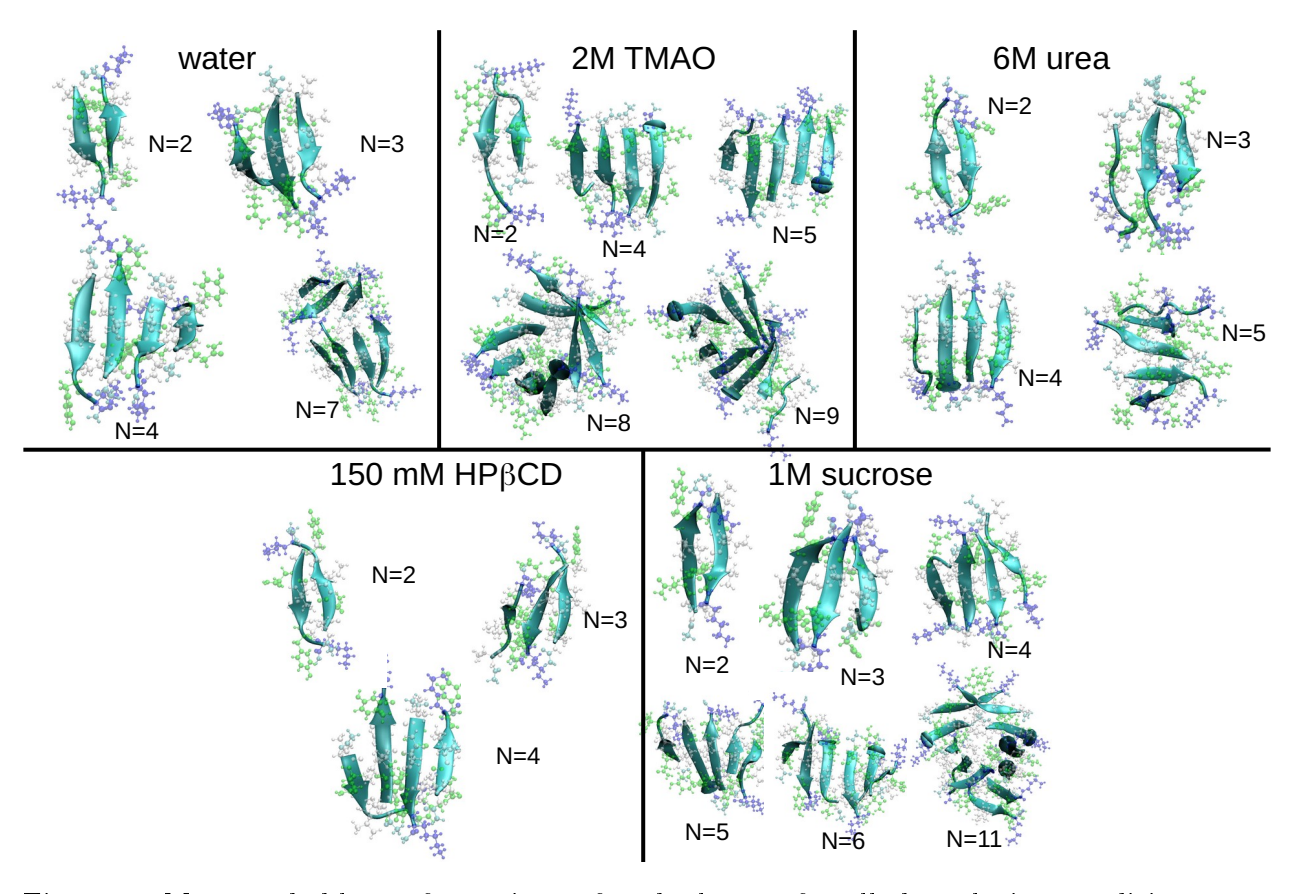


Figure 6: Most probable conformations of each cluster, for all the solution conditions considered. Polar uncharged residues are in green, nonpolar ones in white, positively charged in blue. The set of transfer free energies proposed by Moeser and Horinek⁴⁵ was used for urea.

observed in the hydrogen bonding maps (Figure S3), 1M sucrose stabilized mixed parallel-antiparallel β -strands in clusters N=4, N=5 and N=11. 2M TMAO also promoted the formation of parallel strands in clusters N=4, N=5, N=8 and N=9. In contrast, 6M urea and 150 M HP β CD promoted the formation of antiparallel PHF6 configurations in the most probable conformations. The PHF6 motif forms parallel fibrils *in vitro*, and the higher percentage of parellel configurations promoted by sucrose and TMAO in the oligomers predicted by the simulations may further explain their ability to induce fibrillation.

Conclusions

In the present work, ThT fluorescence and AFM studies have been used to study the fibrillation of PHF6, an aggregation-prone fragment of the Tau protein. PHF6, a hexapeptide located in R3, is considered to be crucial for Tau fibrillation, and constitues the first β -strand of the filament core in Tau filaments isolated from the brain of Alzheimers's disease patients.²⁴ For this reason, clarifying its aggregation pathway is of paramount importance to understand the overall mechanism of fibrillation in the Alzheimer's disease. Molecular dynamics simulations in implicit solvent have also been conducted to provide mechanistic insight into the aggregation pathway of PHF6.

We observed that the extent of aggregation is strongly influenced by the addition of the cosolutes urea, TMAO, sucrose and 2-HP β CD. More specifically, the addition of urea has been shown to significantly hinder the aggregation process, while TMAO promotes fibril formation. This is in line with studies that show a correlation between the levels of TMAO in cerebrospinal fluid and the progression of the Alzheimer's disease. $^{50-52}$ HP β CD is also a potent inhibitor of aggregation, an interesting result considering the widespread use of HP β CD as a drug carrier to the brain and in the treatment of the Niemann-Pick type C disease. Sucrose behaves similarly to TMAO, promoting the formation of ordered aggregates and fibrils.

Overall, molecules with denaturant-like characteristics (urea and 2-HP β CD), that favorably interact with the peptide backbone, inhibit aggregation and promote the monomeric state. The opposite is true in the case of the stabilizing osmolytes TMAO and sucrose, that only weakly interact with the peptide backbone and thereby foster assembly of PHF6.

The simulation approach used in this study gives results that are consistent with the ThT and AFM experimental data. This shows that including free energy of transfer contributions into an implicit solvent description, according to the MIST protocol, represents a powerful approach to reproduce the experimental effect of cosolutes on the aggregation pathway of PHF6. The results discussed in the present manuscript indicate that free-energy based implicit solvent simulations are a valuable approach to study not only conformational changes, but also the aggregation propensity of proteins in different solution conditions. Moreover, molecular simulations have the additional advantage of giving access to a wealth of information, such as the structure of oligomeric states of PHF6 discussed in the present work, that would be inaccessible to current experimental techniques.

Supporting Information

Free energy of transfer values, cluster distribution for the urea-b description, hydrogen bonding maps, secondary structure content, radius of gyration vs. cluster size, asphericity values.

Acknowledgement

The authors acknowledge support from the Center for Scientific Computing at the California Nanosystems Institute (CNSI, NSF grant CNS-1725797) for the availability of high performance computing resources and support. This work used the Extreme Science and Engineering Discovery Environment, which is supported by the National Science Foundation grant number ACI-1548562 (MCA05S027). The authors aknowledge support from the NSF (MCB-1716956, CHE-2107753 (MTB) and CHE-1800352) and the NIH (R01-GM118560-

01A). The authors thank Prof. Songi Han for giving access to the plate reader for the ThT fluorescence assays.

References

- (1) Binder, L. I.; Frankfurter, A.; Rebhun, L. I. The distribution of tau in the mammalian central nervous system. J. Cell Biol. 1985, 101, 1371–1378.
- (2) Grundke-Iqbal, I.; Iqbal, K.; Tung, Y. C.; Quinlan, M.; Wisniewski, H. M.; Binder, L. I. Abnormal phosphorylation of the microtubule-associated protein tau (tau) in Alzheimer cytoskeletal pathology. Proc. Natl. Acad. Sci. 1986, 83, 4913–4917.
- (3) Goedert, M. Tau filaments in neurodegenerative diseases. *FEBS Lett.* **2018**, *592*, 2383–2391.
- (4) Wang, Y.; Mandelkow, E. Tau in physiology and pathology. *Nat. Rev. Neurosci.* **2016**, 17, 22–35.
- (5) Orr, M. E.; Sullivan A, C.; Frost, B. A Brief Overview of Tauopathy: Causes, Consequences, and Therapeutic Strategies. *Trends Pharmacol. Sci.* **2017**, *38*, 637–648.
- (6) Nguyen, P. H.; Ramamoorthy, A.; Sahoo, B. R.; Zheng, J.; Faller, P.; Straub, J. E.; Dominguez, L.; Shea, J.-E.; Dokholyan, N. V.; De Simone, A. et al. Amyloid Oligomers: A Joint Experimental/Computational Perspective on Alzheimer's Disease, Parkinson's Disease, Type II Diabetes, and Amyotrophic Lateral Sclerosis. Chem. Rev. 2021, 121, 2545–2647.
- (7) Nguyen, P. H.; Derreumaux, P. Structures of the intrinsically disordered Aβ, tau and α-synuclein proteins in aqueous solution from computer simulations. Biophys. Chem. 2020, 106421.

- (8) Qi, R.; Wei, G.; Nussinov, R.; Ma, B. Biophysics and Biochemistry of Protein Aggregation; World Scientific: Singapore, 2017; Chapter 2, pp 51–71.
- (9) Goedert, M.; Spillantini, M. G. Propagation of Tau aggregates. *Mol. Brain* **2017**, *10*, 18.
- (10) Lee, G.; Cowan, N.; Kirschner, M. The primary structure and heterogeneity of tau protein from mouse brain. *Science* **1988**, *239*, 285–288.
- (11) Goedert, M.; Spillantini, M. G.; Potier, M. C.; Ulrich, J.; Crowther, R. A. Cloning and sequencing of the cDNA encoding an isoform of microtubule-associated protein tau containing four tandem repeats: differential expression of tau protein mRNAs in human brain. *Embo J.* **1989**, *8*, 393–399.
- (12) Weismiller, H. A.; Murphy, R.; Wei, G.; Ma, R., B. Nussinov; Margittai, M. Structural disorder in four-repeat Tau fibrils reveals a new mechanism for barriers to cross-seeding of Tau isoform. J. Biol. Chem. 2018, 293, 17336–17348.
- (13) von Bergen, M.; Friedhoff, P.; Biernat, J.; Heberle, J.; Mandelkow, E.-M.; Mandelkow, E. Assembly of τ protein into Alzheimer paired helical filaments depends on a local sequence motif (³⁰⁶VQIVYK³¹¹) forming β structure. Proc. Natl. Acad. Sci. 2000, 97, 5129–5134.
- (14) Nguyen, P. H.; Derreumaux, P. Molecular Dynamics Simulations of the Tau Amyloid Fibril Core Dimer at the Surface of a Lipid Bilayer Model: I. In Alzheimer's Disease. J. Phys. Chem. B 2022, 126, 4849–4856.
- (15) Nguyen, P. H.; Derreumaux, P. Molecular Dynamics Simulations of the Tau R3–R4 Domain Monomer in the Bulk Solution and at the Surface of a Lipid Bilayer Model. *J. Phys. Chem. B* **2022**, *126*, 3431–3438.

- (16) Derreumaux, P.; Man, V. H.; Wang, J.; Nguyen, P. H. Tau R3–R4 Domain Dimer of the Wild Type and Phosphorylated Ser356 Sequences. I. In Solution by Atomistic Simulations. J. Phys. Chem. B 2020, 124, 2975–2983.
- (17) Li, X.; Dong, X.; Wei, G.; Margittai, M.; Nussinov, R.; Ma, B. The distinct structural preferences of tau protein repeat domains. *Chem. Commun.* **2018**, *54*, 5700–5703.
- (18) Stohr, J.; Wu, H.; Nick, M.; Wu, Y.; Bhate, M.; Condello, C.; Johnson, N.; Rodgers, J.; Lemmin, T.; Acharya, S. et al. A 31-Residue Peptide Induces Aggregation of Tau's Microtubule-Binding Region in Cells. Nat. Chem. 2017, 9, 874-881.
- (19) Quinn, J. P.; Corbett, N. J.; Kellett, K. A. B.; Hooper, N. M. Tau Proteolysis in the Pathogenesis of Tauopathies: Neurotoxic Fragments and Novel Biomarkers. J. Alzheimer's Dis. 2018, 63, 13–33.
- (20) Peterson, D. W.; Zhou, H.; Dahlquist, F. W.; Lew, J. A Soluble Oligomer of Tau Associated with Fiber Formation Analyzed by NMR. *Biochemistry* **2008**, *47*, 7393–7404.
- (21) Li, W.; Lee, V. M.-Y. Characterization of Two VQIXXK Motifs for Tau Fibrillization in Vitro. *Biochemistry* **2006**, *45*, 15692–15701.
- (22) KrishnaKumar, V.; Paul, A.; Gazit, E.; Segal, D. Mechanistic insights into remodeled Tau-derived PHF6 peptide fibrils by Naphthoquinone-Tryptophan hybrids. Sci. Rep. 2018, 8, 71.
- (23) Zou, Y.; Guan, L.; Tan, J.; Qi, B.; Wang, Y.; Zhang, Q.; Sun, Y. Atomistic Insights into the Inhibitory Mechanism of Tyrosine Phosphorylation against the Aggregation of Human Tau Fragment PHF6. J. Phys. Chem. B 2023, 127, 335–345.
- (24) Fitzpatrick, A. W. P.; Falcon, B.; Shaoda, H.; Murzin, A. G.; Murshudov, G.; Gar-

- ringer, H. J.; Crowther, R. A.; Ghetti, B.; Goedert, M.; Scheres, S. H. W. Cryo-EM structures of tau filaments from Alzheimer's disease. *Nature* **2017**, *547*, 185–190.
- (25) Chen, D.; Drombosky, K. W.; Hou, Z.; Sari, L.; Kashmer, O. M.; Ryder, B. D.; Perez, V. A.; Woodard, D. R.; Lin, M. M.; Diamond, M. I. et al. Tau local structure shields an amyloid-forming motif and controls aggregation propensity. *Nat. Comm.* 2019, 10, 2493.
- (26) Eisenberg, D.; Jucker, M. The Amyloid State of Proteins in Human Diseases. *Cell.* **2012**, *148*, 1188–1203.
- (27) Zheng, X.; Wu, C.; Liu, D.; Li, H.; Bitan, G.; Shea, J.-E.; Bowers, M. T. Mechanism of C-Terminal Fragments of Amyloid β-Protein as Aβ Inhibitors: Do C-Terminal Interactions Play a Key Role in Their Inhibitory Activity? J. Phys. Chem. B 2016, 120, 1615–1623.
- (28) Andreasen, M.; Skeby, K.; Zhang, S.; Nielsen, E.; Klausen, L.; Frahm, H.; Christiansen, G.; Skrydstrup, T.; Dong, M.; Schiøtt, B. et al. The Importance of Being Capped: Terminal Capping of an Amyloidogenic Peptide Affects Fibrillation Propensity and Fibril Morphology. *Biochemistry* **2014**, *53*, 6968–6980.
- (29) Ganguly, P.; Do, T. D.; Larini, L.; LaPointe, N. E.; Sercel, A. J.; Shade, M. F.; Feinstein, S. C.; Bowers, M. T.; Shea, J.-E. Tau Assembly: The Dominant Role of PHF6 (VQIVYK) in Microtubule Binding Region Repeat R3. J. Phys. Chem. B 2015, 119, 4582–4593.
- (30) Eschmann, N. A.; Georgieva, E. R.; Ganguly, P.; Borbat, P. P.; Rappaport, M. D.; Akdogan, Y.; Freed, J. H.; Shea, J.-E.; Han, S. Signature of an aggregation-prone conformation of tau. *Sci. Rep.* **2017**, *7*, 44739.
- (31) Onufriev, A.; Bashford, D.; Case, D. A. Exploring protein native states and large-scale

- conformational changes with a modified generalized born model. *Proteins* **2004**, *55*, 383–394.
- (32) Arsiccio, A.; Ganguly, P.; Shea, J.-E. A Transfer Free Energy Based Implicit Solvent Model for Proteins Simulations in Solvent Mixtures: Urea-Induced Denaturation as a Case Study. J. Phys. Chem. B 2022, 126, 4472–4482.
- (33) Auton, M.; Bolen, D. W. Predicting the energetics of osmolyte-induced protein folding/unfolding. *Proc. Natl. Acad. Sci.* **2005**, *102*, 15065–15068.
- (34) Auton, M.; Rösgen, J.; Sinev, M.; Holthauzen, L. M. F.; Bolen, D. W. Osmolyte effects on protein stability and solubility: A balancing act between backbone and side-chains. *Biophys. Chem.* **2011**, *159*, 90 – 99.
- (35) Serno, T.; Carpenter, J. F.; Randolph, T. W.; Winter, G. Inhibition of Agitation-Induced Aggregation of an IgG-Antibody by Hydroxypropyl-β-Cyclodextrin. J. Pharm. Sci. 2010, 99, 1193–1206.
- (36) Tavornipas, S.; Tajiry, S.; Hirayama, F.; Arima, H.; Uekama, K. Effects of Hydrophilic Cyclodextrins on Aggregation of Recombinant Human Growth Hormone. *Pharm. Res.* **2004**, *21*, 2369–2376.
- (37) Serno, T.; Härtl, E.; Besheer, A.; Miller, R.; Winter, G. The Role of Polysorbate 80 and HPβCD at the Air-Water Interface of IgG Solutions. *Pharm. Res.* **2013**, *30*, 117–130.
- (38) Serno, T.; Geidobler, R.; Winter, G. Protein stabilization by cyclodextrins in the liquid and dried state. Adv. Drug Deliv. Rev. 2011, 63, 1086–1106.
- (39) Davis, M. E.; Brewster, M. E. Cyclodextrin-based pharmaceutics: past, present and future. *Nat. Rev. Drug Discov.* **2004**, *3*, 1023–1035.
- (40) Yancey, P.; Clark, M.; Hand, S.; Bowlus, R.; Somero, G. Living with water stress: evolution of osmolyte systems. *Science* **1982**, *217*, 1214–1222.

- (41) Yancey, P. H. Organic osmolytes as compatible, metabolic and counteracting cytoprotectants in high osmolarity and other stresses. *J. Exp. Biol.* **2005**, *208*, 2819–2830.
- (42) Cho, S. S.; Reddy, G.; Straub, J. E.; Thirumalai, D. Entropic Stabilization of Proteins by TMAO. J. Phys. Chem. B 2011, 115, 13401–13407.
- (43) Schneck, E.; Horinek, D.; Netz, R. R. Insight into the Molecular Mechanisms of Protein Stabilizing Osmolytes from Global Force-Field Variations. J. Phys. Chem. B 2013, 117, 8310–8321.
- (44) Lee, J. C.; Timasheff, S. N. The stabilization of proteins by sucrose. J. Biol. Chem. 1981, 256, 7193–7201.
- (45) Moeser, B.; Horinek, D. Unified Description of Urea Denaturation: Backbone and Side Chains Contribute Equally in the Transfer Model. J. Phys. Chem. B 2014, 118, 107– 114.
- (46) Auton, M.; Holthauzen, L. M. F.; Bolen, D. W. Anatomy of energetic changes accompanying urea-induced protein denaturation. *Proc. Natl. Acad. Sci.* **2007**, *104*, 15317–15322.
- (47) Ganguly, P.; Polák, J.; van der Vegt, N. F. A.; Heyda, J.; Shea, J.-E. Protein Stability in TMAO and Mixed Urea-TMAO Solutions. *J. Phys. Chem. B* **2020**, *124*, 6181–6197.
- (48) O'Brien, E. P.; Okamoto, Y.; Straub, J. E.; Brooks, B. R.; Thirumalai, D. Thermodynamic Perspective on the Dock-Lock Growth Mechanism of Amyloid Fibrils. J. Phys. Chem. B 2009, 113, 14421–14430.
- (49) Xu, R.; Wang, Q. Towards understanding brain-gut-microbiome connections in Alzheimer's disease. *BMC Syst. Biol.* **2016**, *10*, 63.
- (50) Praveenraj, S. S.; Sonali, S.; Anand, N.; Tousif, H. A.; Vichitra, C.; Kalyan, M.; Kanna, P. V.; Chandana, K. A.; Shasthara, P.; Mahalakshmi, A. M. et al. The Role of a

- Gut Microbial-Derived Metabolite, Trimethylamine N-Oxide (TMAO), in Neurological Disorders. *Mol. Neurobiol.* **2022**, *59*, 6684–6700.
- (51) Vogt, N. M.; Romano, K. A.; Darst, B. F.; Engelman, C. D.; Johnson, S. C.; Carlsson, C. M.; Asthana, S.; Blennow, K.; Zetterberg, H.; Bendlin, B. B. et al. The gut microbiota-derived metabolite trimethylamine N-oxide is elevated in Alzheimer's disease. Alz. Res. Therapy 2018, 10, 124.
- (52) Gao, Q.; Wang, Y.; Wang, X.; Fu, S.; Zhang, X.; Wang, R.-T.; Zhang, X. Decreased levels of circulating trimethylamine N-oxide alleviate cognitive and pathological deterioration in transgenic mice: a potential therapeutic approach for Alzheimer's disease. *Aging* **2019**, *11*, 8642–8663.
- (53) Rankin, C. A.; Gamblin, T. C. Assessing the toxicity of tau aggregation. *J. Alzheimers Dis.* **2008**, *14*, 411–416.
- (54) Arya, S.; Ganguly, P.; Arsiccio, A.; Claud, S. L.; Trapp, B.; Schonfeld, G. E.; Liu, X.; Lazar Cantrell, K.; Shea, J.-E.; Bowers, M. T. Terminal Capping of an Amyloidogenic Tau Fragment Modulates Its Fibrillation Propensity. J. Phys. Chem. B 2020, 124, 8772–8783.
- (55) Qiu, D.; Shenkin, P. S.; Hollinger, F. P.; Still, W. C. The GB/SA Continuum Model for Solvation. A Fast Analytical Method for the Calculation of Approximate Born Radii. J. Phys. Chem. A 1997, 101, 3005–3014.
- (56) Bradley, D. J.; Pitzer, K. S. Thermodynamics of electrolytes. 12. Dielectric properties of water and Debye-Hueckel parameters to 350°C and 1 kbar. *J. Phys. Chem.* **1979**, 83, 1599–1603.
- (57) Arsiccio, A.; Shea, J.-E. Protein Cold Denaturation in Implicit Solvent Simulations: A Transfer Free Energy Approach. J. Phys. Chem. B 2021, 125, 5222–5232.

- (58) Hasel, W.; Hendrickson, T. F.; Still, W. C. A rapid approximation to the solvent accessible surface areas of atoms. *Tetrahedron Comput. Methodol.* **1988**, *1*, 103–116.
- (59) Kollman, P. A.; Dixon, R.; Cornell, W.; Fox, T.; Chipot, C.; Pohorille, A. Computer Simulation of Biomolecular Systems, Vol. 3; van Gunsteren, W F and Weiner, P K and Wilkinson, A J (Eds.): Elsevier, Amsterdam, Netherlands, 1997; pp 83–96.
- (60) Pearlman, D. A.; Case, D. A.; Caldwell, J. W.; Ross, W. S.; Cheatham, T. E.; De-Bolt, S.; Ferguson, D.; Seibel, G.; Kollman, P. AMBER, a package of computer programs for applying molecular mechanics, normal mode analysis, molecular dynamics and free energy calculations to simulate the structural and energetic properties of molecules. Comput. Phys. Commun. 1995, 91, 1 41.
- (61) Tribello, G. A.; Bonomi, M.; Branduardi, D.; Camilloni, C.; Bussi, G. PLUMED 2: New feathers for an old bird. *Comput. Phys. Commun.* **2014**, *185*, 604 613.
- (62) Shell, M. S.; Ritterson, R.; Dill, K. A. A Test on Peptide Stability of AMBER Force Fields with Implicit Solvation. *J. Phys. Chem. B* **2008**, *112*, 6878–6886.
- (63) Ilitchev, A. I.; Giammona, M. J.; Olivas, C.; Claud, S. L.; Lazar Cantrell, K. L.; Wu, C.; Buratto, S. K.; Bowers, M. T. Hetero-oligomeric Amyloid Assembly and Mechanism: Prion Fragment PrP(106–126) Catalyzes the Islet Amyloid Polypeptide β-Hairpin. J. Am. Chem. Soc. 2018, 140, 9685–9695.
- (64) Humphrey, W.; Dalke, A.; Schulten, K. VMD: Visual molecular dynamics. J. Mol. Graph. 1996, 14, 33 38.
- (65) Ryckaert, J.-P.; Ciccotti, G.; Berendsen, H. J. Numerical integration of the cartesian equations of motion of a system with constraints: molecular dynamics of n-alkanes. *J. Comput. Phys.* **1977**, *23*, 327 341.

- (66) Wang, A.; Bolen, D. W. A Naturally Occurring Protective System in Urea-Rich Cells: Mechanism of Osmolyte Protection of Proteins against Urea Denaturation. *Biochemistry* 1997, 36, 9101–9108.
- (67) Auton, M.; Bolen, D. W. Additive transfer free energies of the peptide backbone unit that are independent of the model compound and the choice of concentration scale.

 Biochemistry 2004, 43, 1329–1342.
- (68) Auton, M.; Bolen, D. W.; Rösgen, J. Structural thermodynamics of protein preferential solvation: Osmolyte solvation of proteins, aminoacids, and peptides. *Proteins* 2008, 73, 802–813.
- (69) Arsiccio, A.; Rospiccio, M.; Shea, J.-E.; Pisano, R. Force Field Parameterization for the Description of the Interactions between Hydroxypropyl-β-Cyclodextrin and Proteins. J. Phys. Chem. B 2021, 125, 7397–7405.
- (70) Frishman, D.; Argos, P. Knowledge-based protein secondary structure assignment. *Proteins* **1995**, *23*, 566–579.
- (71) Arsiccio, A.; Ganguly, P.; La Cortiglia, L.; Shea, J.-E.; Pisano, R. ADD Force Field for Sugars and Polyols: Predicting the Additivity of Protein-Osmolyte Interaction. J. Phys. Chem. B 2020, 124, 7779-7790.
- (72) Timasheff, S. N. Protein-solvent Preferential Interactions, Protein Hydration, and the Modulation of Biochemical Reactions by Solvent Components. Proc. Natl. Acad. Sci. U.S.A. 2002, 99, 9721 – 9726.
- (73) Kolb, M.; Botet, R.; Jullien, R. Scaling of Kinetically Growing Clusters. *Phys. Rev. Lett.* **1983**, *51*, 1123–1126.
- (74) Isella, L.; Drossinos, Y. Langevin agglomeration of nanoparticles interacting via a central potential. *Phys. Rev. E* **2010**, *82*, 011404.

Graphical TOC Entry

